

SDSS IV MaNGA - Gas Rotation Velocity lags in the Final Sample of MaNGA Galaxies

Dmitry Bizyaev^{1,2,3*}, Rene A. M. Walterbos⁴, Yan-Mei Chen^{5,6}, Niv Drory⁷, Richard R. Lane⁸,

Joel R. Brownstein⁹, Rogemar A. Riffel^{10,11}

¹Apache Point Observatory and New Mexico State University, Sunspot, NM, 88349

²Sternberg Astronomical Institute, Moscow State University, Universitetskii prosp. 13, Moscow, 119234

³Special Astrophysical Observatory of the Russian AS, 369167, Nizhnij Arkhyz

⁴New Mexico State University, Las Cruces, NM, 88003, USA

⁵School of Astronomy and Space Science, Nanjing University, Nanjing 210093, China

⁶Key Laboratory of Modern Astronomy and Astrophysics (Nanjing University), Ministry of Education, Nanjing 210093, China

⁷McDonald Observatory, The University of Texas at Austin, 1 University Station, Austin, TX 78712, USA

⁸Centro de Investigación en Astronomía, Universidad Bernardo O'Higgins, Avenida Viel 1497, Santiago, Chile

⁹Department of Physics and Astronomy, University of Utah, 115 S. 1400 E., Salt Lake City, UT 84112, USA

¹⁰Departamento de Física, CCNE, Universidade Federal de Santa Maria, 97105-900, Santa Maria, RS, Brazil

¹¹Laboratório Interinstitucional de e-Astronomia - LIneA, Rua Gal. José Cristino 77, Rio de Janeiro, RJ - 20921-400, Brazil

Accepted XXX. Received YYY; in original form ZZZ

ABSTRACT

We consider the largest sample of 561 edge-on galaxies observed with integral field units by the MaNGA survey and find 300 galaxies where the ionised gas shows a negative vertical gradient (lag) in its rotational speed. We introduce the stop altitude as the distance to the galactic midplane at which the gas rotation should stop in the linear approximation. We find correlations between the lags, stop altitude and galactic mass, stellar velocity dispersion and overall Sersic index. We do not find any correlation of the lags or stop altitude with the star formation activity in the galaxies. We conclude that low mass galaxies ($\log(M_*/M_\odot) < 10$) with low Sersic index and with low stellar velocity dispersion possess a wider "zone of influence" in the extragalactic gas surrounding them with respect to higher mass galaxies that have a significant spherical component. We estimated the trend of the vertical rotational gradient with radius and find it flat for most of the galaxies in our sample. A small subsample of galaxies with negative radial gradients of lag has an enhanced fraction of objects with aged low surface brightness structures around them (e.g. faint shells), which indicates that noticeable accretion events in the past affected the extraplanar gas kinematics and might have contributed to negative radial lag gradients. We conclude that an isotropic accretion of gas from the circumgalactic medium plays a significant role in the formation of rotation velocity lags.

Key words: galaxies: ISM, galaxies: kinematics and dynamics, galaxies: structure, galaxies: spiral

1 INTRODUCTION

Ionized gas is found not only close to the midplane, but also can be seen at high altitudes in our Galaxy (Hoyle & Ellis 1963; Reynolds 1971; Reynolds et al. 1973, 1999; Shull et al. 2009) as well as in other galaxies (Dettmar 1990; Rand et al. 1990; Rand 1997; Hoopes et al. 1999; Rand 2000; Rossa et al. 2004) (Rossa & Dettmar 2003; Wu et al. 2014), at several kpc from the galactic midplane. The high-altitude gas plays important role for the matter circulation in galaxies (Putman et al. 2012). It may replenish the in-plane gas and support star formation process.

There are different scenarios of the origin of the extra-planar gas. Accretion from the external intergalactic medium not connected to the inner galactic gas is one of them (Oort 1970; White & Rees 1978; Binney 2005; Kaufmann et al. 2006; Combes 2014). Galactic fountains recycle galactic gas and cause its accretion later (Shapiro & Field 1976; Bregman 1980; Norman & Ikeuchi 1989; Marinacci et al. 2011; Fraternali et al. 2013; Lehner et al. 2022; Marasco et al. 2022). These effects do not exclude each other and can play together (Haffner et al. 2009; Benjamin 2012).

As it has been noticed for several nearby galaxies, the gas rotation deviates from cylindrical and sometimes we observe rotation velocity lag. The lags were noticed in atomic (Swaters et al. 1997; Matthews & Wood 2003; Zschaechner et al.

* E-mail: dmbiz@apo.nmsu.edu

2011; Gentile et al. 2013; Kamphuis et al. 2013; Zschaechner & Rand 2015; Zschaechner et al. 2015) and in ionized gas (Fraternali et al. 2004; Heald et al. 2006a,b, 2007; Kamphuis et al. 2007, 2011; Rosado et al. 2013; Wu et al. 2014; Boettcher et al. 2016).

A strong correlation between star formation per unit disc area and the existence of ionized extra planar gas has been noticed (Dettmar 2004; Ho et al. 2016). Contrary to expectations that lags are connected to the star formation activity in galaxies, an inverse correlation between the star formation rate and the lag amplitude was reported by Heald et al. (2007). Zschaechner et al. (2011) did not confirm it. A large sample of edge-on galaxies observed by the MaNGA (Bundy et al. 2015) survey was investigated by Bizyaev et al. (2017) and no connection between the star formation and the lags was found. This result was also confirmed by Levy et al. (2019) with CALIFA (Sanchez et al. 2016) survey data.

Correlation of lags with galactic properties can reveal the nature of the extraplanar ionized gas. Thus, Zschaechner & Rand (2015) reported negative radial gradients of the lags (i.e. the magnitude of the lag decreases toward the periphery of the disc), which points towards the galactic fountains as the main source of the extraplanar gas. Studying HI velocity fields in nearby galaxies in the frames of the HALOGAS project revealed galactic fountains as good explanation for the lags in nearby late-type galaxies (Marasco et al. 2019). On the other hand, Levy et al. (2019) do not find systematic lags in their sample of galaxies and conclude that the main source of the extraplanar gas is an external accretion. The gas accretion from the CGM is a necessary component for explaining kinematics of ionized and neutral gas around galaxies according to Fraternali et al. (2007); Fraternali & Binney (2008); Marinacci et al. (2010), even in the presence of galactic fountains.

To this date, three large Integral Field Unit surveys have been finished (CALIFA¹, Sanchez et al. (2016), MaNGA², Bundy et al. (2015); Abdurroúf et al. (2021), and SAMI³, Allen et al. (2015)) and released their final data. They provide an excellent opportunity for studying the ionized gas in galaxies and around them, as well as its connection to the environment of galaxies (Bloom et al. 2018).

In this paper we utilize the data from the MaNGA survey released at the end of 2021 (Abdurroúf et al. 2021). We concentrate on edge-on galaxies only, which helps minimize projection effects in the galaxies and select regions populated with extraplanar gas only. We called the vertical gradient of rotation velocity as lag throughout the paper.

2 THE FINAL DATA RELEASE OF MANGA

This year the SDSS⁴ has issued the final release of MaNGA panoramic spectroscopy data for 10,010 unique galaxies in the frames of SDSS-IV (Blanton et al. 2017). MaNGA is a massive spectroscopic survey performed with IFU technique (Bundy et al. 2015; Drory et al. 2015), which was run on the

Sloan 2.5 m telescope at Apache Point Observatory (Gunn et al. 2006; Smee et al. 2013). The survey employs a simple, "flat" target selection by stellar mass of the galaxies (Wake et al. 2017). MaNGA uses 17 IFUs simultaneously with size from 12 to 32 arcsec (19 to 127 fibers, respectively), see Drory et al. (2015). The precision of the flux calibration is at the level of a percent (Yan et al. 2016), with the best spectral resolution $\sigma \sim 25 \text{ km s}^{-1}$ (Law et al. 2021). The median redshift of the survey's object is about 0.03 (Law et al. 2016). The final MaNGA data release provides raw reduced spectra (Law et al. 2016) as well as numerous high-level products such as maps of gas and stellar kinematics, spectral indices, fluxes in individual emission lines, and many others (Westfall et al. 2019; Abdurroúf et al. 2021).

2.1 Edge-on Galaxies observed by MaNGA

Following the approach by Bizyaev et al. (2017, B17 hereafter), we visually inspected SDSS images of all MaNGA galaxies. The objects we considered to be true edge-on galaxies if they did not show spiral arms and had a dust lane projected very close to the galactic disc midplane and nucleus. We were able to identify 561 edge-on galaxies.

2.2 Edge-on Galaxies with Regular Lags

Following B17, we plotted radial velocity profiles for selected galaxies drawn parallel to the minor axis and searched for regularly descending velocities with the distance to midplane. We used the H α emission velocity maps and only the spaxels with the signal-to-noise ratio SNR>3 and without bad processing flags set by the data reduction pipelines. As a result we selected 300 edge-on galaxies with regular rotation velocity lags. SDSS images of the galaxies are shown on Figure 1.

¹ Calar Alto Legacy Integral Field spectroscopy Area survey

² Mapping Nearby Galaxies at Apache Point Observatory

³ Sydney-Anglo-Australian Observatory Multi-object Integral field survey

⁴ Sloan Digital Sky Survey, <http://sdss.org>

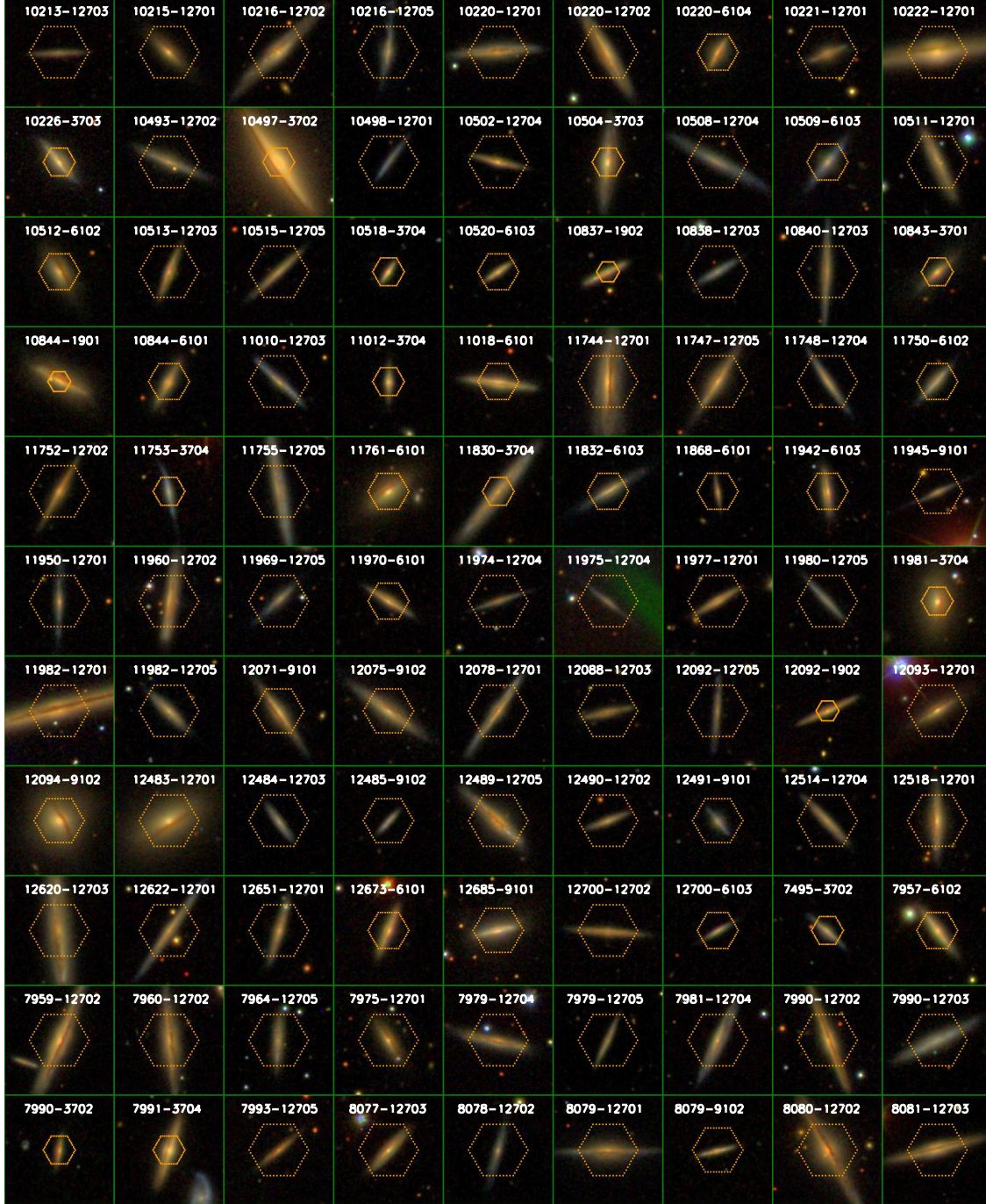


Figure 1. SDSS images of selected edge-on galaxies with regular rotation curve lags. All images show 1 arcmin x 1 arcmin square area. The yellow contours designates the MaNGA IFU allocation.

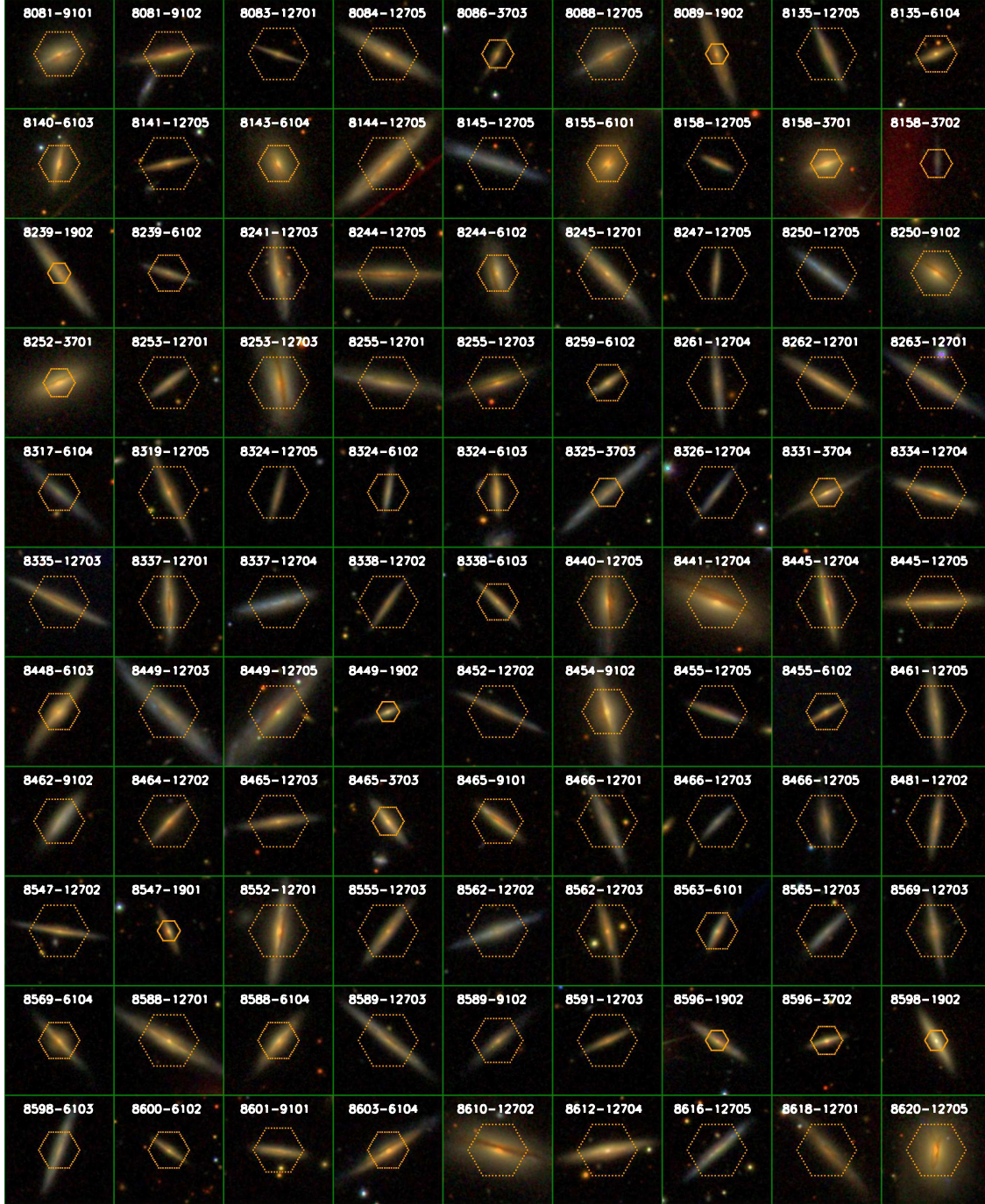


Figure 1. Continue of Fig. 1

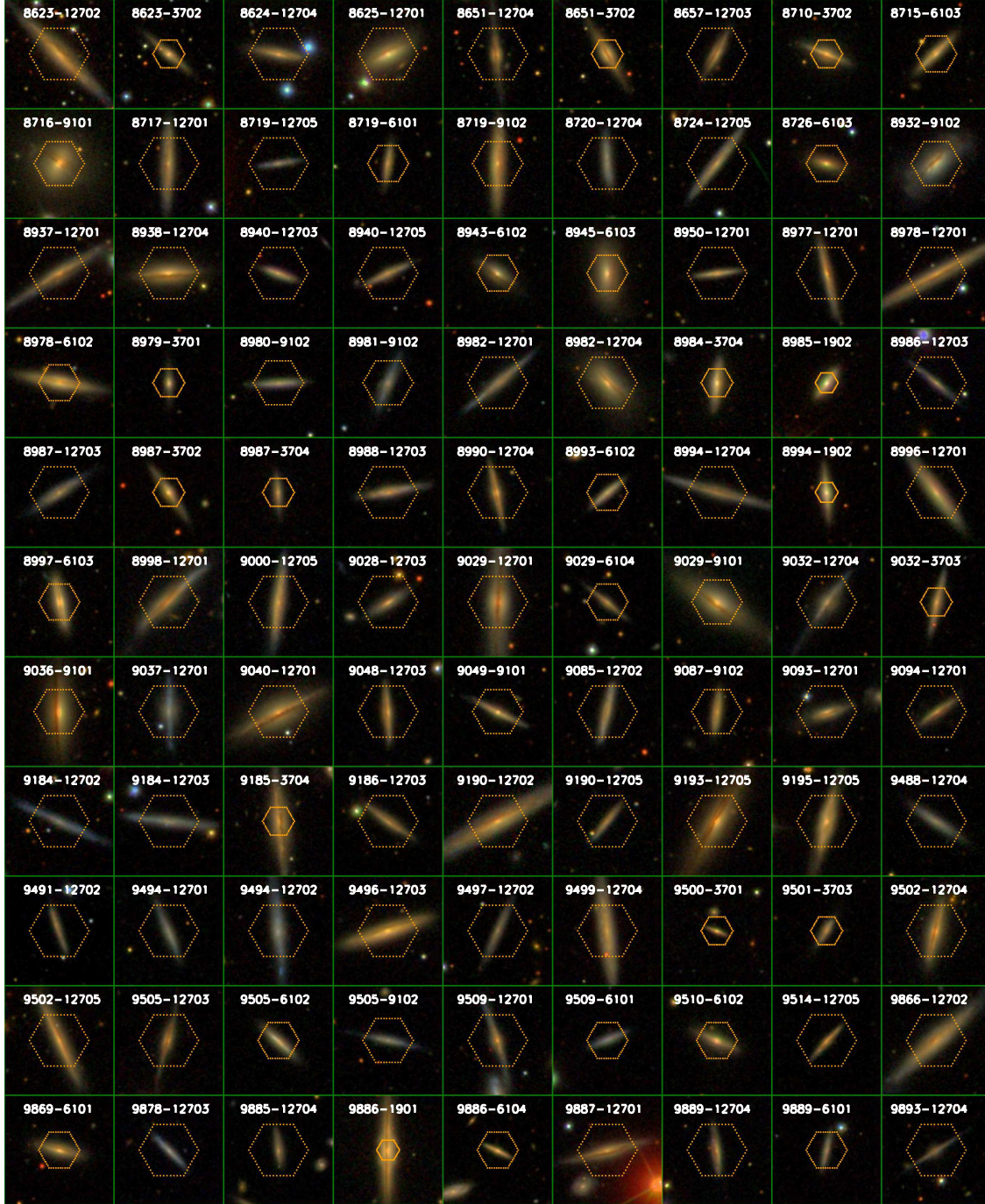


Figure 1. Continue of Fig. 1

3 IONIZED GAS VELOCITY FIELDS

3.1 Modelling Velocity Fields with Lags

We use benefits of two-dimensional velocity fields provided by panoramic spectroscopy and compare them to the same model used in B17. The model assumes that the $H\alpha$ emission follows an exponential distribution along the radial and vertical directions in the discs. We estimate the radial and vertical scales of for $H\alpha$ maps made with the MaNGA data cubes and the same procedure as in Bizyaev & Mitronova (2002); Bizyaev et al. (2014). The rotation curve is parameterized via a simple function with a linear raising part at the centre, see B17. The three-dimensional distribution of the velocities is projected on the sky plane by integrating along the line of sight. The dust extinction is taken into account in the model via introducing a co-planar exponential dust disc. Similar to B17, the dust disc has the same spatial scales as the gas disc, and the central extinction of the dust is a free parameter of the model. Finally, the projected radial velocity maps are convolved with a gaussian kernel corresponding to the spatial resolution of MaNGA emission line velocity maps. The convolution uses corresponding $H\alpha$ fluxes as weights. The model parameters are estimated via the chi-square minimization of the difference between the model maps and observations.

Same as in B17, the lag of the rotation is introduced as a vertical gradient of rotation curve: $V(r, z) = V(r) - |z| dv/dz$, where r and z are the radial and vertical coordinates on the sky plane, and V is the projected radial velocity. We have shown (B17) that introducing the lag significantly improves the projects velocity fitting to the observing data if the estimated lag value exceeds a few km s^{-1} .

Figure 2 shows results of our fitting for a typical MaNGA edge-on galaxy. The observed and model velocity fields are shown along with the observed and model rotation curves in the galactic midplane and at 2 kpc above it. Due to the vertical lag in rotational velocities, the amplitude of the rotation curve is lower at high altitude with respect to the midplane.

3.2 Rotation Velocity Lags in the Galaxies

We observe no correlation with star formation activity in our sample of galaxies. We applied two approaches to estimate the star formation rate: via $H\alpha$ luminosity, and via WISE W4 band flux. There is no dependence can be seen in Figure 3: relationships on both left and right top panels have the Pearson correlation coefficient (CC hereafter) of 0.07. We also considered an average star formation density estimated as the integrated $H\alpha$ or W4 fluxes divided by galactic disc area. The area is estimated as $2\pi R_{\text{petro}}^2$, where R_{petro} is the Petrosian disc radius from the parental NASA-Sloan Atlas, Blanton et al. (2011) (NSA⁵) catalog. Lags do not show correlation with the star formation density as well: the bottom panels in Figure 3 correspond to CC = 0.09 and 0.10 for the left and right panels, respectively.

Similar to B17, lags show tendency to be higher for galaxies with large stellar mass and central velocity dispersion, see Figure 4. The correlation coefficient for both panels in Figure 4 is CC = 0.43. The visual ellipticity of the galaxies, as well as their Sersic index "n" weakly correlate with the value

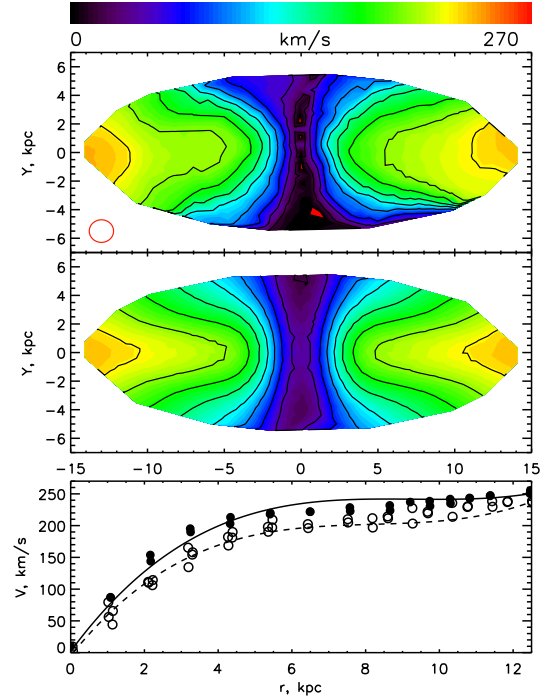


Figure 2. An example of the velocity field fitting, the MaNGA galaxy 1-122111. Top panel: the MaNGA observing velocity field. We show absolute velocities on the plot. The red ellipse at the lower left corner of the panel indicates the MaNGA spatial resolution (sigma). Middle: the model velocity field. Bottom: two observing (bullets) and model (curves) rotation curves in the galactic midplane (filled symbols) and at 2 kpc above the midplane (open symbols).

of lags as well in Figure 5: CC = 0.30 for the upper panel and CC = 0.48 for the lower one.

The emission lines flux in the central spaxel of the galaxies allows to classify them on the BPT diagram (Baldwin et al. 1981; Veilleux & Osterbrock 1987). For consistency with B17, we used the classifications based on SDSS spectroscopic survey spectra, which were estimated independently of MaNGA. The data are taken from the MPA-JHU catalog (Brinchmann et al. 2004). The classes 1 and 2 correspond to star forming and low signal-to-noise star forming regions; class 3 designates composite regions; class 4 shows the AGN (excluding LINERs) nuclei; class 5 corresponds to LINERs. Similar to B17, the galaxies with AGNs and LINERs tend to have larger lags, while galaxies with star-forming nuclei seldom have extraplanar gas with high rotation lag. The lag difference between the classes 1-2 and 4-5 is about 3 times, see Figure 6.

While the lag indicates a gradient of rotation descending, we can formally calculate the distance in the vertical direction that corresponds to a completely stopped rotation, z_{stop} , in the linear approximation. Introducing a spatial scale allows us to eliminate the size effect in the lag trends. We define the stop-altitude as $z_{\text{stop}} = V_{\text{max}}/\text{lag}$, where V_{max} is the maximum rotation velocity. The latter is estimated in our modelling in §3.1. In Figure 7 we consider trends of z_{stop} ,

⁵ <http://nsatlas.org>

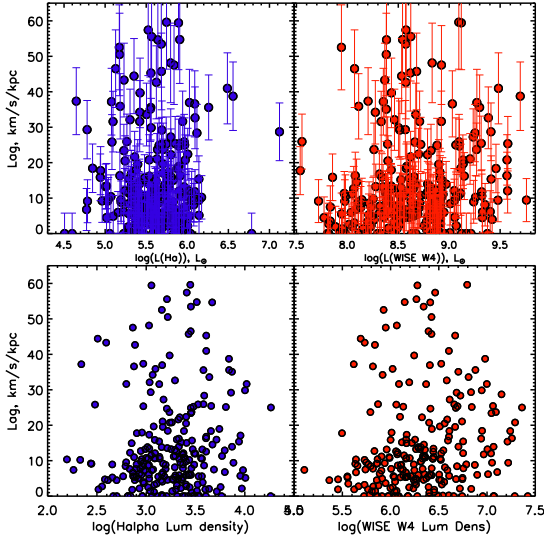


Figure 3. The rotation velocity lag versus the star formation properties in the galaxies: the $H\alpha$ and WISE W4 luminosities (upper row) and their surface density (lower row).

and also of the stop altitude normalized by the scale height of ionized gas estimated as in B17. Similar to Figures 3–5, the absolute and normalized stop-altitude does not show any dependence on the star formation rate or star formation density. At the same time we notice that normalized stop-altitude is significantly shorter for massive galaxies, galaxies with high velocity dispersion and with high Sersic index.

3.3 Radial Gradients of Lags

Following Levy et al. (2019), we consider possible radial variations of lags in the galaxies. We modified the pipeline described in §2.1 and added a possibility of a radial linear variation of the lags. Levy et al. (2019) used CALIFA data obtained for larger than MaNGA galaxies. To ensure that MaNGA data provide sufficient radial resolution, we removed several galaxies in which the MaNGA IFU covers the very central part only. Next, we compared the maximum radial extent of our objects with the resolution element that corresponds to 2.5 arcsec resolution in the final MaNGA maps (Law et al. 2016). It turned out that only a few galaxies in the sample have less than 4 resolution elements coverage from the centre to the edge, while most of selected galaxies have a better coverage. We considered the number of resolution elements per MaNGA data radial extent as a parameter and explored whether the further trends of radial variations of parameters discussed below depend on the parameter. We do not find any dependence on the radial resolution and con-

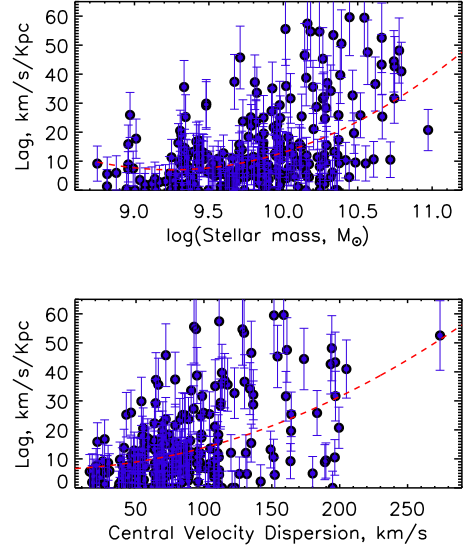


Figure 4. The rotation velocity lag versus the stellar mass (upper) and central stellar velocity dispersion (lower). The red dashed curve is a polynomial regression of the data.

clude that MaNGA radial resolution is sufficient to explore the radial gradients of lags.

The distribution of the radial variation of lags is shown in Figure 8. Most of the galaxies indicate modest radial lag gradients, although a few of them show significant negative gradients. We explore the radial lag gradient trends in Figure 9. The black circles show the measurements in the galaxies, while the red bullets designate the slipping median and median absolute deviation (MAD) uncertainties in the sample. It is seen that the radial lag gradient is essentially zero for all possible galaxy parameters. The gradient bias towards its negative values for massive galaxies with large Sersic index is caused by small statistics in corresponding regions of parameter space.

According to Levy et al. (2019), the radial lag gradient is an indicator of the lag origin. The negative $d\text{lag}/dr$ anticipates a larger lag at the central parts of galaxies than at its periphery due to the ejected gas momentum conservation (Shapiro & Field 1976; Bregman 1980; Fraternali et al. 2007; Fraternali & Binney 2008; Marinacci et al. 2010, 2011). A uniform infall of circumgalactic gas (Binney 2005) or a cylindrical accretion from the galactic corona (Kaufmann et al. 2006) should not cause any lag gradients for the assumption of the accretion uniformity. The gas accretion from the CGM at low inclination angles to the galactic midplane was studied by simulations (Stewart et al. 2011) and was observed in some galaxies (Lehner et al. 2013). The gas accretion via the in-plane inflow redistributes the gas momentum in the disc,

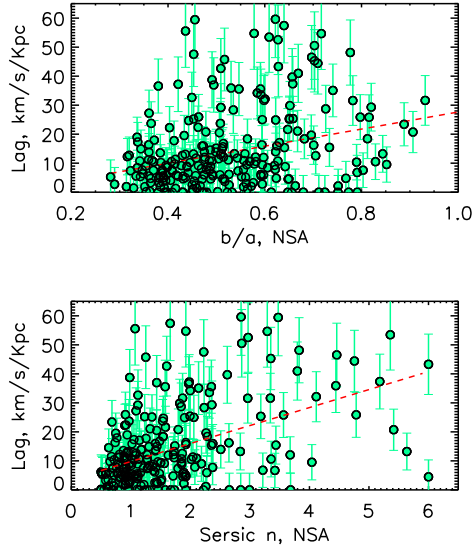


Figure 5. The rotation velocity lag versus the apparent ellipticity of the edge-on galaxies and their Sersic index taken from the NSA catalog. The red dashed curve shows a polynomial regression.

creates larger lags at the galactic periphery, and thus causes positive lag radial gradients (see also [Putman et al. 2012](#); [Combes 2014](#)).

3.4 The Lag asymmetry between different sides of the galaxies

Interaction of galactic gas with circumgalactic medium (CGM) may be affected by non-uniformities of the CGM. Interactions with nearby satellites can also be a factor that affects galactic gas on the opposite sides from the galactic midplane ([Ghosh et al. 2021](#)). Thus, asymmetric interactions may lead to different value of lag estimated above and below the galactic midplane. We use the same approach described in § 3.1 and evaluated the same models for the “upper” and “lower” parts of the edge-on galaxies separately. Then we find the $\Delta(\text{lag})$ as the absolute difference between the lags on the two opposite halves of galaxies (with respect to the midplane). Figure 10 shows the $\Delta(\text{lag})$ as a function of stellar mass, stellar velocity dispersion, star formation rate and Sersic index. We cannot claim any clear linear trends. We notice the lack of large $\Delta(\text{lag})$ values for galaxies with the Sersic n greater than 3, although this area of the parameter space has a small number of data points. Figure 11 shows that there is no correlation between the lags and $\Delta(\text{lag})$.

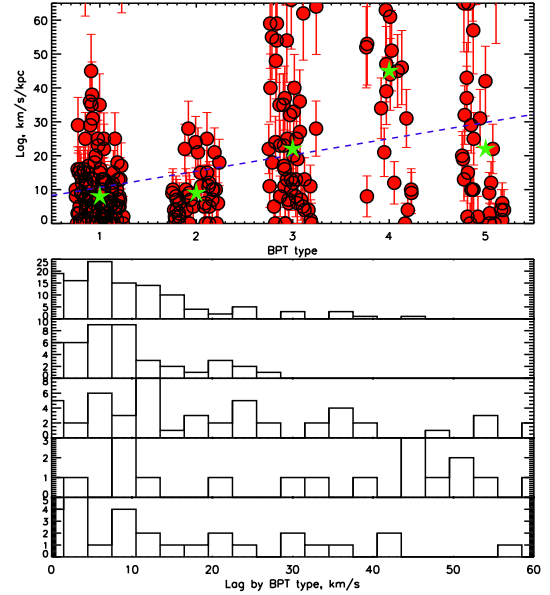


Figure 6. Top: the rotation velocity lag is shown for different BPT classes ([Brinchmann et al. 2004](#)). The classes 1-2 designate objects with emission line ratios from the centre typical for star forming regions. The class 3 marks composite regions. The classes 4 and 5 designate the AGN and LINERs nuclei, respectively. The points are randomly scattered in the X-direction for a better representation. The blue dashed line shows the linear regression. It demonstrates about three times larger lags in the AGN-LINER galaxies with respect to the star forming ones. The green stars designate the median values of the lag in each BPT class. Bottom: each BPT class from the top plot is shown as a separate histogram (class 1 to 5 from top to bottom).

3.5 Environment of Galaxies and the Lag Variation

Since the lag origin is connected to the CGM and the environment of galaxies, we expect that the presence of some environmental structures may correlate with strong rotation velocity lags. We were able to find images of all our galaxies with regular lags in the LEGACY survey sky atlas ([Dey et al. 2019](#)). We visually inspected the outskirts of each galaxy and searched for such elements as low surface brightness shells, loops, bridges, streams, extended spiral arms, envelopes common with other galaxies, and also noticeable asymmetries of external isophotes - in a manner it was classified by ([Atkinson et al. 2013](#)). In addition, we visually inspected extended areas around the galaxies and counted possible satellites around them. We distinguished between small (non-stellar objects without noticeable structure), medium (with smaller size than the studied galaxies), large (comparable to the main galaxy in size), and great satellites (larger than the main object). Since we have no information about redshifts of the satellites in most cases, we expect that many small satellites

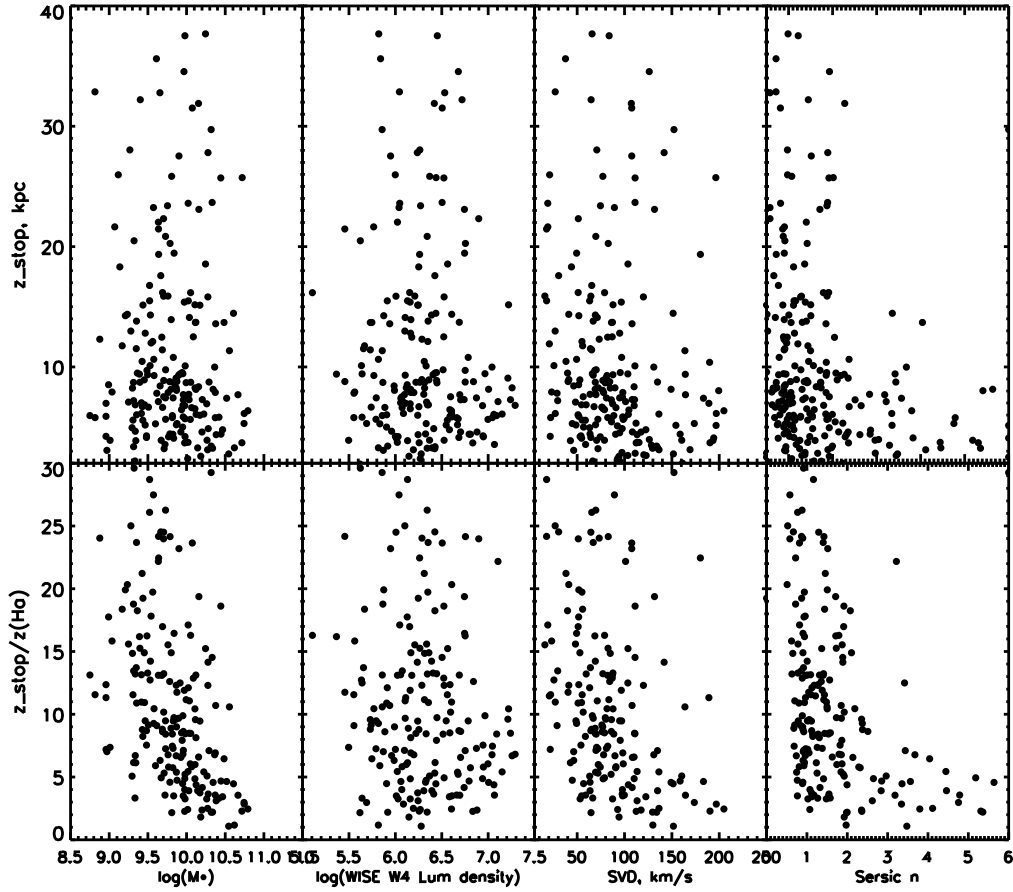


Figure 7. The absolute (upper) and normalized (lower) stop altitude versus the galactic stellar mass, W4 luminosity density, central stellar velocity dispersion, and Sersic index. Note that the formally calculated correlation coefficients for all panels $|CC|$ are less than 0.1, although some non-linear trends can be seen in the bottom panels.

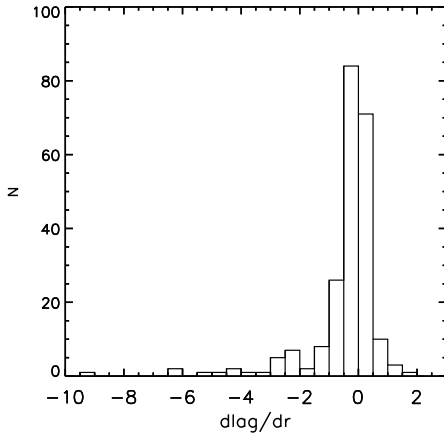


Figure 8. The histogram distribution of the radial gradient of lags. While most of the galaxies show values close to zero, the distribution has a "tail" towards the negative values. The tail ($d\log/dr < -2 \text{ km s}^{-1} \text{ kpc}^{-2}$) contains 8 % of all galaxies. The $2 \text{ km s}^{-1} \text{ kpc}^{-2}$ corresponds to the right limit of the quasi-gaussian centered at the zero value.

are projected objects. At the same time, the medium, and especially large and great satellites have a good chance to be at the same distance as our galaxies.

We compared the number of the medium and larger sizes satellites (according to the classification above) for the galaxies in our sample and did not find significant difference between the objects with large and small lags.

We plot histograms of the lag, lag gradient and lag asymmetry (Δlag) distributions for galaxies with and without two most commonly observed faint features around them: low surface brightness shells and noticeable asymmetry of their external isophotes, see Figure 12. The absence (black line) or presence (red line) of shells (upper panels) and outer asymmetries (lower panels) make some histograms look different. We compare the distributions via the two-sample Kolmogorov-Smirnov (K-S) test. The lags show large difference between the samples (probability of the similarity is $p=0.004$ and 0.130 for the shells and asymmetry, respectively), as well as the lag gradient ($p=0.018$ and 0.130). The lag asymmetry demonstrates a significant similarity for the low surface brightness shells and asymmetry with probabilities $p=0.73$ and 0.84 , respectively.

We classified all identified environmental features around the galaxies by young, intermediate age and old, based on the stage of parental interaction. The structures are called young if they are typical for the starting phase of galactic

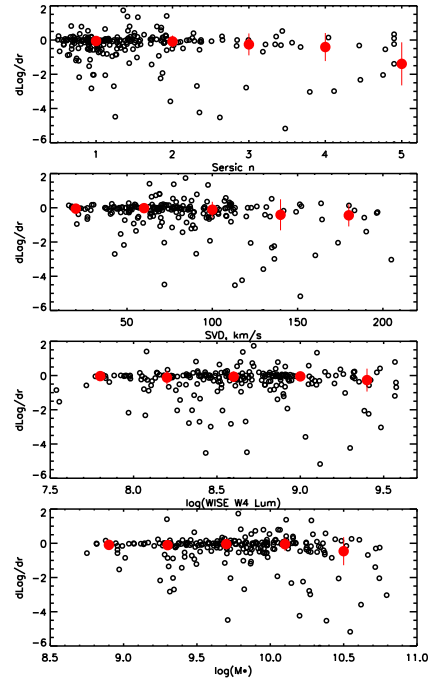


Figure 9. The lag radial gradients in individual galaxies versus their stellar mass, W4 luminosity, stellar velocity dispersion and Sersic index (black circles). The red bullets designate the slipping median values with 1.48 MAD for the error bars.

interaction. We consider bridges, tight group membership, distortion due to an evident interaction, streams, and tidal structures between interacting galaxies as young structures. On the opposite side there are old structures that are smooth and extended in space, e.g. shells, extended loops, inner and outer rings. Formation of those structures requires more than one turn of a satellite around its host galaxy. We consider unusual dust pattern seen in the objects and arcs as structures of intermediate age.

Figure 13 shows histogram distributions of lag, radial gradient of lag and the lag asymmetry Δlag for the young, intermediate and old structures. The presence of the structures is designated with the red lines, while the absence of them with the black. The lag distributions for the objects with young faint structures look rather similar for the K-S test ($p=0.72$), while the intermediate and old structures make difference ($p=0.02$ and 0.07 , respectively). The lag gradients show some similarity for the young structures ($p=0.31$) and difference for the intermediate and old ($p=0.09$ and 0.01 , respectively). The lag asymmetry looks very similar for the young and old features ($p=0.96$ and 0.93 , respectively), while the histograms for intermediate age are similar with $p=0.33$.

4 RESULTS AND DISCUSSION

We confirm general trends of the lag and lag gradient found by Bizyaev et al. (2017) and Levy et al. (2019) with our signif-

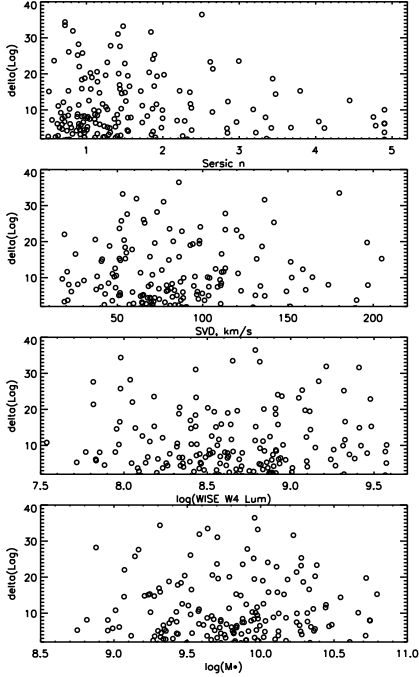


Figure 10. The absolute difference Δlag between the lag estimated for the lower and upper parts of the galaxies versus the general galactic properties: stellar mass, W4 luminosity, stellar velocity dispersion, and Sersic index. The formally calculated correlation coefficients $|CC|$ for all panels above are less than 0.1.

icantly larger sample. We don't find any correlation between the star formation activity (defined by the integrated rate or per unit surface area) in galaxies and their gas rotation lag. The lag value correlates with galactic stellar mass, rotation curve amplitude and central stellar velocity dispersion. The stop altitude introduced in this paper is seen as a proxy for the demarcation between the internal and external gas from the standpoint of its kinematics. When normalized by the scaleheight of ionized gas (Figure 7), the stop altitude suggests that low mass galaxies (stellar mass less than $10^{10} M_{\odot}$) with low Sersic index and stellar velocity dispersion possess a wider "zone of influence" with respect to massive galaxies with a large contribution of spheroidal component. From scaling up size with mass in galaxies and by assuming the same density of surrounding circumgalactic gas, we could expect to see more extended "zone of influence" of internal gas in massive galaxies with respect to low mass objects. Our Figure 7 shows the opposite. This, in turn, points at a difference in the properties of gas surrounding low- and high-mass galaxies and suggests that interaction between the internal and external gas plays a critical role in the formation of lags - at least in a majority of the galaxies in our MaNGA edge-on sample.

At the same time, the lag radial gradient is found negative in a small fraction of all galaxies, as shown in Figure 8. According to Levy et al. (2019) and references therein, the

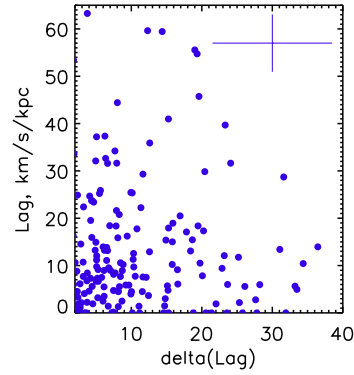


Figure 11. Comparison of the lag and Δlag . The typical error bars are shown in the upper right corner of the plot.

negative radial gradients point at the internal origin of lags and their connection to galactic fountains. We see noticeable negative gradients in only 8 % of our galaxies, see Figure 8. There is no particular mass, Sersic index, or star formation rate range correlated with the radial lags. Our results do not indicate that the lags caused by galactic fountains are ubiquitous or can be predicted from some general galactic properties. Instead, most of the galaxies demonstrate negligible radial gradients of lags, consistent with a gas accretion scenario (Levy et al. 2019). Note that the vertical lags generally have been found too large to be explained purely with galactic fountain models and that accretion has been suggested (Fraternali et al. 2007; Fraternali & Binney 2008; Marinacci et al. 2010).

The lag asymmetry, defined as a difference between the lag determined on both sides from the galactic midplane independently, does not show a significant correlation with general galactic properties (Figure 10).

Our study of galactic environment shows that some stellar low surface brightness structures can be seen more often in galaxies with larger lags. According to Figure 11, low surface brightness shells and outer isophote asymmetry are more frequently observed in galaxies with large lags and with significant negative radial lag gradients. At the same time, these faint structures do not depend on the lag asymmetry.

When interaction-borne environmental structures are subdivided by young, intermediate, and old based on their typical age of interaction coarsely determined from the structure extension and geometry, the lag and radial lag gradient his-

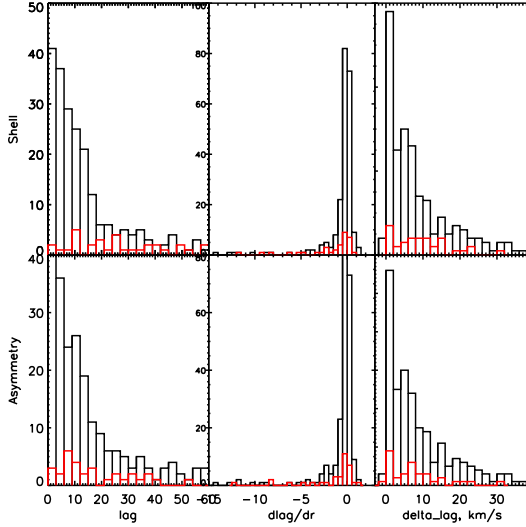


Figure 12. The histogram distributions of the lag, lag radial gradient $d\log/dr$ and Δlag for the galaxies with (red) and without (black) shells (upper panels) and asymmetry of external isophotes (lower panels). The probability of similarities of the two samples is $p=0.004$, 0.018 , and 0.73 for the upper panels, and $p=0.130$, 0.130 , and 0.84 for the lower panels, see text.

ogram distributions are significantly different between the samples with and without the old environmental structures around. The sample with the old structures around is biased towards the objects with large lags and negative lag gradients, see Figure 13. The young structures around the galaxies do not affect their lag and lag radial gradient distributions. We cautiously avoid from making conclusions for the intermediate age structures because of poor statistics in this case. Our results suggest that we observe significant coincidence of old environmental structures and the high frequency of large lags and negative radial lag gradients in galaxies. Similar to the case of galactic fountains scenario when the expelled gas returns back to its host galaxy, interaction with galactic environment, which is often accompanied by the gas infall, causes large radial lag gradients. As it can be seen in Figure 13, the gas infall that took place in the past increases the amplitude of lags and causes negative lag radial gradients. At the same time, for most of our galaxies we do not observe significant radial gradients of lags, and also we don't find any connection between the lag asymmetry and past interaction events. This allows us to reject the gas accretion caused by interaction with satellites scenario for most of the galaxies. In turn, it favours the gas accretion from the CGM as the main source of rotation velocity lags - same conclusion as reported in a

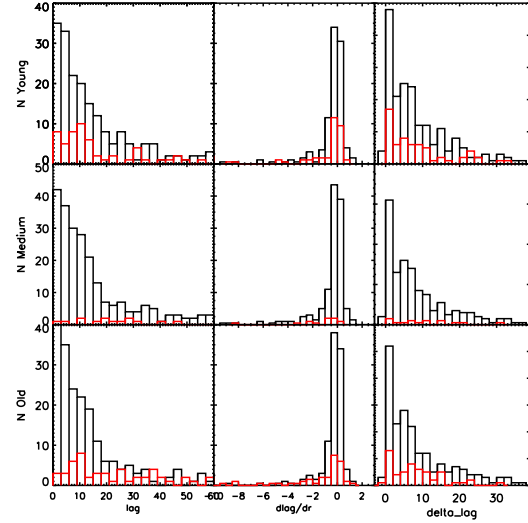


Figure 13. The histogram distributions of the lag, lag radial gradient $d\log/dr$ and Δlag for the galaxies with (red) and without (black) Young (upper panels), Intermediate (middle panels) or Old (lower panels) low surface brightness structures around them. The probability of similarities of the two samples is $p=0.72$, 0.31 , and 0.96 for the upper row, $p=0.02$, 0.09 , and 0.33 for the middle row, and $p=0.07$, 0.01 , and 0.93 for the lower panels, see text.

recent, similar study by [Levy et al. \(2019\)](#), but with a much larger sample.

5 CONCLUSIONS

We considered the largest sample of 561 edge-on galaxies observed up to date with integral field units by the MaNGA survey. Among them, 300 galaxies show regular decreasing of their rotation velocity on their ionized gas velocity fields, or simply lag.

We consider how the lags and the stop altitude (defined as the distance at which the gas rotation should stop, in the linear approximation), depend on general properties of galaxies. We do not find any correlation of the lags or stop altitude with the star formation activity in the galaxies. Instead, mild correlations of the stop altitude found in the paper suggest that low mass galaxies with low Sersic index and with low stellar velocity dispersion - the objects that should have a high specific fraction of gas with respect to stars, - possess wide "zone of influence" in the extragalactic gas surrounding them. In contrast, massive galaxies with large contribution of spherical component experience more significant effects from the extragalactic gas which imprints in kinematics of their extraplanar gas.

We estimated the radial gradients of lags and find them flat for most of the galaxies in our sample, which suggests connection between the lags and accretion from the intergalactic media. A small subsample of galaxies with negative radial gradients of lag have enhanced fraction of objects with aged low surface brightness structures around them (e.g. faint shells), which indicates that noticeable satellite accretion events in the past affected the extraplanar gas kinematics and might have caused negative lag gradients.

We considered the lag asymmetry between the "upper" and "lower" parts of the galaxies with respect to galactic mid-planes, and found neither correlation of it with galactic parameters nor its connection to the galactic environment.

Based on the high frequency of zero radial gradient of lag in a combination with low lag asymmetry in most of our galaxies, we conclude that isotropic accretion of gas from the CGM plays a significant role in the formation of gas rotation velocity lags.

ACKNOWLEDGEMENTS

We thank the anonymous referee for constructive feedback that improved the paper. This work is partially supported by the National Science Foundation under Grant No. AST-1615594 to RAMW. Y. C acknowledges support from the National Natural Science Foundation of China (NSFC grants 11573013, 11733002, 11922302). RAR acknowledges partial financial support from CNPq and FAPERGS. The project is partly supported by RSCF grant 19-12-00145. SDSS-IV acknowledges support and resources from the Center for High-Performance Computing at the University of Utah. The SDSS web site is www.sdss.org.

SDSS-IV is managed by the Astrophysical Research Consortium for the Participating Institutions of the SDSS Collaboration including the Brazilian Participation Group, the Carnegie Institution for Science, Carnegie Mellon University, the Chilean Participation Group, the French Participation Group, Harvard-Smithsonian Center for Astrophysics, Instituto de Astrofísica de Canarias, The Johns Hopkins University, Kavli Institute for the Physics and Mathematics of the Universe (IPMU) / University of Tokyo, Lawrence Berkeley National Laboratory, Leibniz Institut für Astrophysik Potsdam (AIP), Max-Planck-Institut für Astronomie (MPIA Heidelberg), Max-Planck-Institut für Astrophysik (MPA Garching), Max-Planck-Institut für Extraterrestrische Physik (MPE), National Astronomical Observatory of China, New Mexico State University, New York University, University of Notre Dame, Observatorio Nacional / MCTI, The Ohio State University, Pennsylvania State University, Shanghai Astronomical Observatory, United Kingdom Participation Group, Universidad Nacional Autónoma de México, University of Arizona, University of Colorado Boulder, University of Oxford, University of Portsmouth, University of Utah, University of Virginia, University of Washington, University of Wisconsin, Vanderbilt University, and Yale University.

DATA AVAILABILITY

This work makes use of SDSS/MaNGA project data publicly available at https://www.sdss.org/dr17/data_access/.

REFERENCES

- Abdurroúf, Accetta K., Aerts C. et al. 2021, ArXiv: 2112.02026
- Alam, Sh., Albareti, F. D., Allende Prieto, C. et al. 2015, *ApJS*, 219, 12
- Allen, J. T., Croom, S. M., Konstantopoulos, I. S. et al. 2015, *MNRAS*, 446, 1567
- Atkinson, A. M., Abraham, R. G., Ferguson, A. M. N. 2013, *AJ*, 765, 28
- Baldwin, J. A., Phillips, M. M., & Terlevich, R., 1981, *PASP*, 93, 5
- Behroozi, P. S., Wechsler, R. H., & Conroy, C. 2013, *ApJ*, 770, 57
- Benjamin, R. A., 2012, *EAS Pub. Ser.*, 56, 299
- Bianchi, S. 2007, *A&A*, 471, 765
- Binney, J. 2005, in *Extra-planar Gas Conference*, ed. R. Braun, *ASP Conf. Ser.*, 331, 131
- Bizyaev, D. & Kajsın, S. 2004, *ApJ*, 613, 886
- Bizyaev, D. & Mitronova, S. 2002, *A&A*, 389, 795
- Bizyaev, D., Kautsch, S., Mosenkov, et al. 2014, *ApJ*, 787, 24
- Bizyaev, D., Walterbos, R. A. M., Yoachim, P. et al. 2017, *ApJ*, 839, 87
- Blanton, M. R., Kazin, E., Muna, D. et al. 2011, *AJ*, 142, 31
- Blanton, M. R., Bershad, M. A., Abolfathi, B. et al., 2017, *AJ*, 154, 28
- Bloom, J. V., Croom, S. M., Bryant, J. J. et al. 2018, *MNRAS*, 476, 2339
- Boettcher, E., Zweibel, E., Gallagher, J. S. III, & Benjamin, R., arXiv:1609.07491
- Bregman, J. N. 1980, *ApJ*, 236, 577
- Brinchmann, J., Charlot, S., White, S. D. M., Tremonti, C. et al. 2004, *MNRAS*, 351, 1151
- Bundy, Kevin; Bershad, Matthew A.; Law, David R.; 2015 *ApJ*, 798, 7
- Collins, J. A., Benjamin, R. A., & Rand, R. J. 2002, *ApJ*, 578, 98
- Combes, F. 2014, in *Astronomical Society of the Pacific Conf. Series*, 480, *Structure and Dynamics of Disk Galaxies*, ed. M. S. Seigar & P. Treuthardt, 211
- de Grijs, R., Peletier, R. F., & van der Kruit, P. C., 1997, *A&A*, 327, 966
- Dettmar, R.-J., 1990, *A&A*, 232, L15
- Dettmar, R.-J., 2004, *Astrophysics and Space Science*, 289, 349
- Dey, A., Schlegel, D. J., Lang, D. et al. 2019, *AJ*, 157, 168
- Drory, N., MacDonald, N., Bershad, M. A., Bundy, K. et al. 2015 *AJ*, 149, 77
- Fraternali, F., Oosterloo, T., & Sancisi, R. 2004, *A&A*, 424, 485
- Fraternali, F., & Binney, J. J., 2006, *MNRAS*, 366, 449
- Fraternali, F., Binney, J., Oosterloo, T. & Sancisi, R. 2007, *New Astronomy Reviews*, 51, 95
- Fraternali, F., & Binney, J. J., 2008, *MNRAS*, 386, 935
- Fraternali, F., Marasco, A., Marinacci, F., & Binney, J., 2013, *ApJ*, 764, 21
- Gentile, G., Jozsa, G. I. G., Serra, P., et al. 2013, *A&A*, 554, 125
- Ghosh, S., Saha, K., Jog, C. J. et al. 2021, arXiv:2105.05270
- Gunn, J. E., Siegmund, W. A., Mannery, E. J. et al. 2006, *AJ*, 131, 2332
- Haffner, L. M., Dettmar, R.-J., Beckman, J. E., Wood, K., et al. 2009, *Rev. Mod. Phys.*, 81, 969
- Heald, G. H., Rand, R. J., Benjamin, R. A., et al. 2006, *ApJ*, 636, 181
- Heald, G. H., Rand, R. J., Benjamin, R. A., Bershad, M. A., 2006, *ApJ*, 647, 1018
- Heald, G. H., Rand, R. J., Benjamin, R. A., Bershad, M. A., 2007, *ApJ*, 663, 933
- Ho, I.-T., Medling, A. M., Bland-Hawthorn, J., Groves, B. et al. 2016, *MNRAS*, 457, 1257
- Hoopes, C. G., Walterbos, R. A. M., Rand, R. J., 1999, *ApJ*, 522, 669
- Hoyle, F. & Ellis, G. R. A. 1963, *Aust. J. Physics*, 16, 1
- Jarrett, T. H., Masci, F., Tsai, C. W., et al., 2013, *AJ*, 145, 6

- Kylafis, N., Misoritis, A., Papamastorakis, J., & Xilouris, E. 2001, *Astrophysics and Space Sci.*, 276, 531
- Kamphuis, P., Peletier, R. F., Dettmar, R.-J., et al. 2007, *A&A*, 468, 951
- Kamphuis, P., Peletier, R. F., van der Kruit, P. C., & Heald, G. H. 2011, *MNRAS*, 414, 3444
- Kamphuis, P., Rand, R. J., & Jozsa, G. I. G. 2013, *MNRAS*, 434, 2069
- Kaufmann, T., Mayer, L., Wadsley, J. et al. 2006, *MNRAS*, 370, 1612
- Law, David R.; Yan, Renbin; Bershad, Matthew A. et al. *AJ*, 150, 19
- Law, D. R., Cherinka, B., Yan, R., Andrews, B. H. et al. 2016, *AJ*, 152, 83
- Law, D. R., Westfall, K. B., Bershad, M. A. et al. 2021, *AJ*, 161, 52
- Lehner, N., Howk, J. C., Tripp, T. et al. 2013, *ApJ*, 770, 138
- Lehner, N., Howk, J. C., Marasco, A. and Fraternali, F. 2022, *MNRAS*, 513, 3228
- Levy, R.C., Bolatto, A.D., Sanchez, S.F. et al. 2019, *ApJ*, 882, 84
- Marasco, A., Fraternali, F., Heald, G. et al. 2019, *A&A*, 631, 50
- Marasco, A., Fraternali, F., Lehner, N., and Howk, J. C. 2022, *arXiv:2202.05852*
- Marinacci, F., Binney, J., Fraternali, F. et al., 2010, *MNRAS*, 404, 1464
- Marinacci, F., Fraternali, F., Nipoti, C. et al. 2011, *MNRAS*, 415, 1534
- Matthews, L. D., Gallagher, J. S., & van Driel, W. 1999, *AJ*, 118, 2751
- Matthews, L. D. & Wood, K. 2003, *AJ*, 593, 721
- Mosenkov, A. V., Sotnikova, N. Ya., Reshetnikov, V. P., Bizyaev, D. et al. 2015, *MNRAS*, 451, 2376
- Nelder, J.A. & Mead, R. 1965, *Computer Journal* 7: 308313
- Norman, C. A. & Ikeuchi, S. 1989, *ApJ*, 345, 372
- Oort, J.H. 1970, *A&A*, 7, 381O
- Putman, M. E., Peek, J.E.G., & Joun, M.R. 2012, *ARA&A*, 50, 491
- Rand, R. J., Kulkarni, S. R., & Hester, J. J. 1990, *ApJ*, 352, L1
- Rand, R. J. 1997, *ApJ*, 474, 129
- Rand, R. J. 2000, *ApJ*, 537, L13
- Relaño, M., Lisenfeld, U., et al. 2007, *ApJ*, 667, L14
- Reynolds, R. J. 1971, PhD Thesis (The University of Wisconsin - Madison)
- Reynolds, R. J., Scherb, F. & Roesler, F. L. 1973, *ApJ*, 185, 869
- Reynolds, R. J., Haffner, L. M., & Tufte, S. L. 1999, in *New Perspectives on the Interstellar Medium*, ed. A. R. Taylor, T. L. Landecker, & G. Joncas, *ASP Conf. Ser.*, 168, 149
- Rosado, M., Gabbasov, R. F., Repetto, P., et al. 2013, *AJ*, 145, 135
- Rossa, J. & Dettmar, R.-J. 2003, *A&A*, 406, 493
- Rossa, J., Dettmar, R.-J., Walterbos, R. A. M., & Norman, C. A. 2004, *AJ*, 128, 674
- Sanchez, S. F., Garcia-Benito, R., Zibetti, S. et al. 2016, *arxiv:160402289S*
- Shapiro, P. R. & Field, G. B. 1976, *ApJ*, 205, 762
- Shull, M.J., Jones, J.R., Danforth, C.W., & Collins, J.A. 2009, *ApJ*, 699,754, 2009
- Smee, S. A., Gunn, J. E., Uomoto, A. et al. 2013, *AJ*, 146, 32
- Stewart, K., Kaufmann, T., Bullock, J. et al. 2011, *ApJ*, 738, 39
- Swaters, R. A., Sancisi, R., & van der Hulst, J. M. 1997, *ApJ*, 491, 140
- Veilleux, S. & Osterbrock, D. E. 1987, *ApJ*, 63, 295
- Wake, D. A., Bundy, K., Diamond-Stanic, A. et al. 2017, 154, 86
- Westfall, K. B., Cappellari, M., Bershad, M. A. et al. *AJ*, 158, 31
- White, S. D. M. & Rees, M. J. 1978, *MNRAS*, 183, 341
- Wright, E. L., Eisenhardt, P. R. M., Mainzer, A. K. et al. 2010, *AJ*, 140, 1868
- Wu, C. J., Walterbos, R. A., Rand, R. J. et al. *American Astronomical Society, AAS Meeting* 223, 453.19
- Xilouris, E. M., Byun, Y. I., Kylafis, N. D., et al. 1999, *A&A*, 344, 868
- Yan, Renbin; Tremonti, Christy; Bershad, Matthew A. et al. 2016, 151, 8
- Yoachim, P. & Dalcanton, J. J. 2006, *AJ*, 131, 226
- Zhu, Y.-N., Wu, H., Cao, C., & Li, H.-N., 2008, *ApJ*, 686, 155
- Zschaechner, L. K. & Rand, R. J. 2015, *ApJ*, 808, 153
- Zschaechner, L. K., Rand, R. J., Heald, G. H., et al. 2011, *ApJ*, 740, 35
- Zschaechner, L. K., Rand, R. J., Walterbos, R. A. M., 2015, *ApJ*799, 61

This paper has been typeset from a \LaTeX file prepared by the author.